Journal of Structural Geology, Vol. 15, No. 9/10, pp. 1189 to 1205, 1993
Printed in Great Britain

0191-8141/93 $06.00+0.00

Lattice preferred orientations and microstructures of deformed Cordilleran marbles: correlation of shear indicators and determination of strain path

B. G. ERSKINE, F. HEIDELBACH and H.-R. WENK

Department of Geology and Geophysics, University of California, Berkeley, CA 94720, U.S.A.

(*Received* 30 *June* 1992; *accepted in revised form* 17 *February* 1993)

Abstract—Marbles from nine Cordilleran deformation zones (the Raft River and Snake Ranges, the Ruby, Rincon and Riverside Mountains, the eastern Peninsular Ranges mylonite zone, and three sites in the Death Valley region) were sampled for microstructural analysis of thin and ultra-thin sections and pole figure measurements by X-ray diffraction to interpret their deformation history.

Microstructural observations reveal various degrees of recrystallization. Fabrics are predominantly symmetric, but some samples display consistent asymmetries of the long grain axes (schistosity) and the macroscopic foliation plane defined by compositional layering. These asymmetric microstructures are most pronounced in non-recrystallized fabrics.

Well-developed textures are found at all sites with *c*-axes perpendicular to the foliation and *a*-axes in a girdle in the foliation plane. The sense of shear derived from slightly asymmetric $\{11\bar{2}0\}$ pole figures is consistent with the shear sense determined in the field and by *S*–*C* structures in adjacent gneisses. The magnitude of the obliquity of $\{11\bar{2}0\}$ girdles suggests that the component of simple shear is relatively small even in samples with highly asymmetric microstructures. We conclude that the obliquity of the $\{11\bar{2}0\}$ girdles is a reliable indicator of the strain path during the last substantial increment of strain and indicates that the carbonate rocks studied deformed dominantly in pure shear. This implied strain path for carbonate rocks may not necessarily reflect the regional strain path, because strain may be partitioned between rocks of different compositions, or between zones of predominantly pure and simple shear at all scales.

INTRODUCTION

THE Cordilleran metamorphic core complexes (Coney 1973) are located within a broad N–S-trending belt of Cenozoic deformation at the western border of cratonal North America (e.g. Crittenden *et al.* 1980, Armstrong 1982) (Fig. 1). The main common characteristics of these structures are a crystalline basement that is overlain by a sequence of sedimentary or metasedimentary rocks, and a detachment fault that separates the two units from each other. The basement (lower plate) is generally Precambrian to Cambrian and commonly intruded by plutonic rocks of various ages. The amount of deformation in the basement increases upwards toward the décollement zone which is characterized by a low-angle normal fault. The deformational characteristics give evidence of both ductile and brittle behavior of the rocks. The upper plate rocks generally consist of blocks of Paleozoic and/or Mesozoic miogeoclinal sedimentary rocks which have been tilted along listric normal faults.

The deformation history of the décollement zone (whether it is mainly contractional or extensional), has been a matter of debate. Most authors today agree on an extensional deformation event during Tertiary time that generally decreases in age from Eocene in the northern Cordillera to Miocene in the south (Coney 1980). The direction of extension is predominantly outward from the tectonic axes of the Mesozoic fold and thrust belt (Wust 1986). Two main types of extensional deformation histories have been suggested. The first is a 'pure shear' model involving symmetrical extension of the crust and implying relatively small displacements on the décollement zone, which is thought to represent an uplifted brittle–ductile transition of the upper crust (Rehrig & Reynolds 1980, Miller *et al.* 1983, Gans & Miller 1984, Lee *et al.* 1987). The second is a 'simple-shear' model that interprets the décollement zone as an extended shear horizon which has its roots in the lower crust and displays high amounts of actual displacement (Wernicke 1981, 1983, Wernicke & Burchfiel 1982, Davis 1983). The activity of the shear horizon from lower to upper crustal levels causes the coexistence of both brittle and ductile deformational features in the movement zone. Lister & Davis (1989) proposed a model in which the décollement zone (as a large shear zone) nucleated in a ductile pure shear zone of the lower crust.

In this study we try to elucidate the problem of the deformation path by microstructural and textural analysis of strongly deformed marbles from a number of well-studied Cordilleran deformation zones, most of them mylonitized basement of different core complexes. The carbonate rocks as mechanically weak parts of the mylonite sequences play an important role in characterizing the strain and kinematic history. Theoretical modelling of calcite deformation based on polycrystal plasticity and comparison with experimentally produced textures gives us a basis for interpreting patterns of preferred orientation. Wenk *et al.* (1987) used it to determine the relative amount of pure and simple shear (i.e. the degree

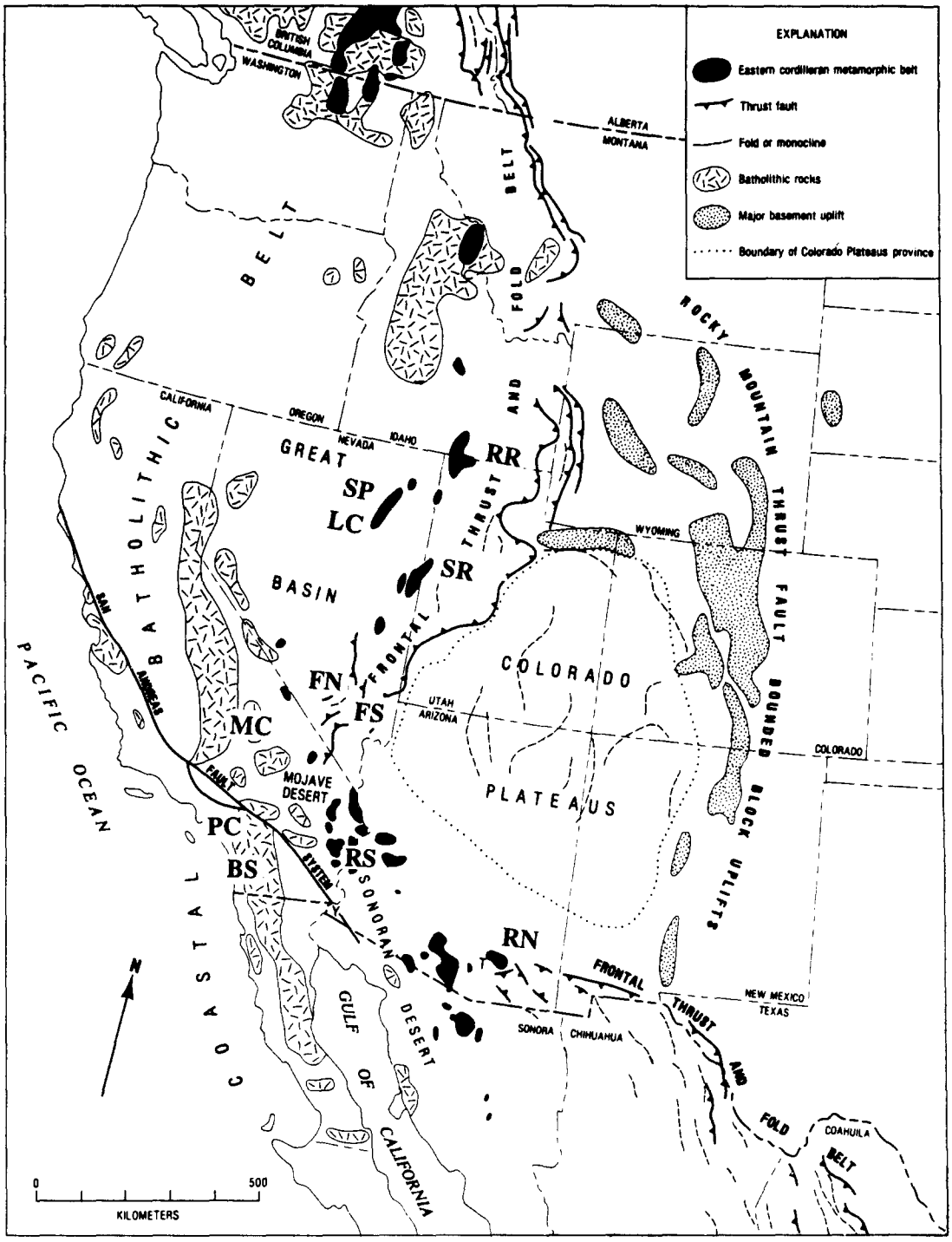

Fig. 1. Map of western North America with core complexes and sample sites (from Haxel *et al.* 1984). RR, Raft River; SP, LC; Ruby Mountains; SR, Snake Ranges; RN, Rincon Mountains; RS, Riverside Mountains; BS, PC, Eastern Peninsular Ranges; FN, FS, MC, Death Valley Region.

of non-coaxial deformation) from the obliquity of the (0001) maximum, or the $\{11\bar{2}0\}$ great circle girdle in pole figures relative to the macroscopic foliation plane. Microstructural indicators such as those described by White *et al.* (1980), Dietrich & Song (1983), Simpson & Schmid (1983) and Lister & Snoke (1984) are also useful in analyzing the deformation history.

The samples were collected from nine different sites, five of these located in various core complexes (Snake Range, Raft River, Ruby Mountains, Rincon Mountains and Riverside Mountains). We also sampled the eastern Peninsular Ranges mylonite zone (Borrego Springs and Palm Canyon) and two other sites in the Death Valley region (Funeral Mountains, Panamint Range) which are not as thoroughly studied and added here as test cases.

DESCRIPTIONS OF THE SAMPLE LOCALITIES

A short description of the local geology for each sample site is given in the following section. The geo-

Table 1. Geographic co-ordinates of the sample sites

Sample site	Longitude	Latitude
Raft River (RR)	113°34'10"W	41°52'00"N
Ruby Mountains, Secret Pass (SP)	115°14'50"W	40°50'26"W
Ruby Mountains Lamoille Canyon (LC)	115°27'13"W	40°41'40"N
Snake Ranges (SR)	114°29'30"W	39°29'30"N
Rincon Mountains (RN)	110°27'44"W	32°11'17"N
Riverside Mountains (RS)	114°30'12"W	34°02'13"N
Eastern Peninsular Ranges, Borrego Springs (BS)	116°23'10"W	33°18'20"N
Eastern Peninsular Ranges, Palm Canyon (PC)	116°29'41"W	38°22'10"N
Death Valley Region, Funeral Mountains North (FN)	116°53'10"W	36°39'20"N
Death Valley Region Funeral Mountains South (FS)	116°45'00"W	36°17'30"N
Death Valley Region, Panamint Ranges (MC)	117°09'30"W	36°34'32"N

graphic co-ordinates of each sample locality are given in Table 1 (see also Fig. 1).

Raft River Range (RR)

The Raft River Ranges consist of a broad autochthon overlain by two major allochthonous sheets separated by low-angle décollements (Compton 1975, 1980). Deformation in the autochthon increases upward; the core is characterized by relatively undeformed Precambrian granitic rocks which become more gneissic toward the décollement. Farther upward the rock grades into a mica schist which is capped by the strongly deformed Elba quartzite. Deformation was progressive and episodic, beginning in Mesozoic (Jurassic?) time and continuing throughout uplift and cooling at about 20 Ma (Compton *et al.* 1977). The high symmetry of quartz *c*-axis pole figures and field data is interpreted by Compton (1980) as reflecting regional pure shear deformation with local moderate components of simple shear.

We collected samples within a relatively narrow (5–6 m thick) carbonate unit in the autochthon just below the fault separating it from the allochthonous sheet. The consistency in the orientation of the macroscopic foliation and lineation within the marble, gneissic rocks below the carbonates, and within quartzite above the fault suggest that the fabric of the marble has not been modified by brittle deformation associated with faulting. Shear indicators in the quartz-bearing rocks were observed to indicate a top-to-the-west sense of displacement, parallel to the SSW-trending stretching lineation. This shear sense is consistent with early displacements on the low-angle faults as suggested by field evidence (Compton 1980).

Ruby Mountains (LC,SP)

The Ruby Mountains expose a diverse sequence of Paleozoic miogeoclinal strata that have been metamorphosed to upper amphibolite facies grade, migmatized and recumbently folded (Howard 1980). The dominant structure is the W-dipping Lamoille Canyon nappe which folds the Prospect Mountain quartzite and the marble of Verdi Peak, as well as the pre-metamorphic Ogilvie thrust fault that originally duplicated these units. The core of the nappe is characterized by high-grade metasedimentary rocks that are intermixed with leucocratic garnet two-mica pegmatitic granite and other granitic rocks. The migmatic core grades upward into a transition zone characterized by a diverse group of mylonitic rocks that contain a regionally consistent NNW-trending stretching lineation. Where exposed on the western flank of the range, these rocks have been greatly attenuated and thinned to as much as only 5% of their original thickness. Deformation of the migmatitic core, the transition zone, and recumbent folding were previously thought to be coeval (Jurassic?) (Howard 1966, 1968, 1980, Snoke 1980); however, recent studies suggest that mylonitization may be younger (Oligocene–Miocene, Snoke & Howard 1984). Lister & Snoke (1984) proposed that the mylonite zone records a major ductile shear zone formed by regional extension.

We sampled two localities. The first site (LC) is located near the mouth of Lamoille Canyon within the mylonite rocks discussed above (south of field stop 1, Snoke & Howard 1984). Samples were collected from fine-grained marble that is strongly foliated and contains a well-developed stretching lineation that trends nearly E–W. Structural analysis of disharmonic folds near this site and *S–C* relationships in mylonitic Prospect Mountain quartzite across Lamoille Canyon indicate a top-to-the-WNW sense of shear (Snoke & Howard 1984). This shear sense is corroborated by asymmetric fabrics in mylonitic gneiss adjacent to the marble outcrops.

The second sampling site (SP) is located in the northern tip of the range at Secret Pass (field stop 12, Snoke & Howard 1984). Samples were collected from the Horse Creek assemblage which is separated from an underlying schistose–quartzite gneiss unit by a low-angle normal fault. Shear criteria in quartz-bearing rocks below the fault indicate a top-to-the-WNW sense of shear parallel to the regional stretching lineation. It is presumed, based on field evidence, that the rocks above the fault were deformed with, and have the same shear sense as the rocks below. In contrast to the excellent samples found in Lamoille Canyon, marble in the Horse Creek assemblage is less deformed. The macroscopic foliation associated with mylonitic carbonate rocks is only moderately developed at best, and stretching lineations are uncommon.

Snake Range (SR)

A classic example of geologic relations that characterizes Cordilleran metamorphic core complexes is found in the Snake Range, Nevada. Supracrustal rocks extended by normal faults are separated from ductilely deformed igneous and metamorphic rocks by a subhorizontal brittle discontinuity called the Snake Range décollement (Miller *et al.* 1983). The upper plate is composed of Middle Cambrian to Permian sedimentary rocks and 35 Ma old volcanic rocks that are juxtaposed along normal faults. The rocks have rotated 'domino-style' so that fault blocks are separated by low-angle faults. In contrast, rocks beneath the décollement are flat-lying, not cut by faults, and thinned 30–90%. These lower plate rocks possess a penetrative, subhorizontal foliation and a regionally consistent WNW stretching lineation. Geologic data, including shear indicators and the analysis of symmetric to asymmetric quartz c-axis pole figures, suggest that the Snake Ranges décollement represents the ductile–brittle transition, and that rocks below this discontinuity have been deformed in pure shear which was followed by simple shear with a top-to-the-east sense of displacement (Miller *et al.* 1983, Gans & Miller 1984, Lee *et al.* 1987).

Samples were collected from the marble mylonite ledge below the Snake Ranges décollement at two localities. The first site is in Rock Canyon near the type locality of the Snake Range décollement (field stop 14, Gans & Miller 1984, field stop 2, Miller *et al.* 1987). The second site is on the ridge south of Hendry's Creek west of the small klippe (west of field stop 15, Gans & Miller 1984, field stop 3, Miller *et al.* 1987). Sampling at these sites was complicated by presence of brittle fractures presumably associated with the décollement overlying these rocks, and an earlier foliation, which is generally not transposed entirely into the regional foliation. Samples collected for this study possess a well-developed penetrative foliation and stretching lineation that is identical in trend to the regional lineation found in the underlying Prospect Mountain quartzite.

Rincon Mountains (RN)

The Rincon Mountains east of Tucson, Arizona, have a basement of granitic Catalina Gneiss which is topped by the Catalina fault. The fault is frequently marked by a zone of chloritic breccia and interpreted as a low-angle normal fault (Davis 1975). The upper plate units consist of folded sedimentary and metasedimentary rocks of Paleozoic and Mesozoic age, which were strongly folded and transposed due to gravity sliding during a mid-Tertiary extensional deformation (Frost 1977). Shear indicators reveal a movement of the upper plate to the southwest (Lingrey 1982).

The sample for this study was taken from the Bear Creek area in the northeastern part of the Rincon Mountains. Paleozoic metasediments consisting mainly of calcitic rocks dip moderately to the southeast and rest concordantly on the gneissic basement. A zone of chloritic breccia is not present.

Riverside Mountains (RS)

The Riverside Mountains in the southeastern part of California display two structural units separated by a low angle normal fault (Lyle 1982). The lower unit is characterized by strongly deformed Paleozoic and Mesozoic metasediments interleaved with Precambrian crystalline rocks. Dominant structures are NE–SW-striking thrust faults which are interpreted as the result of Mesozoic contractional deformation (Lyle 1982). The upper unit consists of rotated blocks of Tertiary volcanic and clastic rocks that rest discordantly on Precambrian basement and are disrupted by normal faults.

The samples for this study were taken from strongly deformed Permian Kaibab limestone in the northeastern area of the Riverside Mountains (near Mountaineer Mine). The limestone is a member of the Paleozoic series in the lower plate and close to the detachment fault in the sampled area. The rocks dip moderately to the northeast and the relative movement of the upper plate during extension was northeastward.

Eastern Peninsular Ranges mylonite zone (BS, PC)

The eastern Peninsular Ranges mylonite zone consists of strongly deformed plutonic rocks and metasedimentary tectonites on the eastern flank of the northern Peninsular Ranges batholith, southern California. Based on shear criteria, which indicate an east-over-west sense of shear, Simpson (1984) provided evidence for Sharp's (1979) proposal that the mylonite zone represents an exposure of a deeply seated thrust belt. This has been questioned by Erskine & Wenk (1985) who thought that the simple shear component may have been overemphasized. Not only marble textures but also quartz textures in mylonite of the granodiorite protolith are surprisingly symmetrical (Wenk & Pannetier 1990). While there is no doubt that *S–C* structures consistently suggest an east-over-west sense of shear (e.g. Simpson & Schmid 1983, O'Brien *et al.* 1987), deformed xenoliths in Palm Canyon lack asymmetry with respect to the macroscopic foliation. Deformation in all the structural units and along the post-mylonitic faults appears to be related to the late Cretaceous–early Cenozoic convergence and to the emplacement of the Peninsular Ranges batholith (Erskine 1986, Todd *et al.* 1988, Goodwin & Renne 1991).

Two sites were sampled within the mylonite zone. The first (BS) is located in Borrego Palm Canyon west of Borrego Springs at an outcrop of metasedimentary rocks within the mylonite zone. The marble at this site is strongly foliated and lineated, and displays reclined folds with fold axes transposed into coincidence with the stretching lineation (sheath folds). The second locality (PC) in the Palm Canyon Formation is on the east flank of Palm Canyon (Palm Springs). Marble in this structural unit is strongly deformed, possesses a well-

developed foliation and stretching lineation that is coincident with the underlying mylonite zone, and includes rootless reclined sheath folds.

Death Valley Region, southeastern California (MC, FN, FS)

The Death Valley region of southeastern California is a part of the Basin and Range Province that has experienced large-scale crustal extension since at least early Miocene time. The upper crustal extension has been accommodated in part by low-angle normal faults with many of the characteristics associated with ' Metamorphic Core Complexes' (Coney 1980). Two areas within this region were sampled. The first is a locality in Mosaic Canyon (MC) in the northern Panamint Ranges at Tucki Mountain in deformed carbonate rocks within a series of low-angle detachment faults. The geology of this area has been mapped in detail (Wernicke *et al.* 1986), and many of the geologic relations have been evaluated. The rocks from Mosaic Canyon are metacarbonate rocks of the Noonday Dolomite exposed beneath the Mosaic Canyon fault (see fig. 2, field stop 6 of Wernicke *et al.* 1986). The Mosaic Canyon fault has a thick (up to 300 m) zone of fault gouge and breccia, and places unmetamorphosed Stirling Quartzite and Bonanza King Formation above greenschist facies rocks below. Mesostructures in the Noonday rocks are very tight reclined folds with a crenulation lineation, open inclined folds, 'tension' fractures and ductile normal faults. The rocks of interest here are strongly deformed calcitic carbonates with a well-defined planar fabric and stretching lineation that post-dates the other ductile structures in the area. These rocks generally dip gently to the north or northeast, and possess a lineation that trends to the north. Shear-sense indicators such as asymmetric folds, *S–C* type relationships, and asymmetric tension crack fillings are mostly well developed, and indicate a top-to-the-north sense of shear.

The second area was sampled at two sites: the western flank of the Funeral Mountains east of the Tucki Mountain site (FN, FS). Little is known about the geologic relations of the carbonate rocks. They were mainly selected to test the techniques that are applied in this study and may be used to gain information in areas that have not received much attention. FN was taken at the Keane Wonder Mine located north of Beatty Junction in Death Valley and FS near Mormon Point. The rocks in this area dip gently southward and are generally broadly folded with a fold axis that trends southeast. Parallel to this fold axis is a penetrative stretching lineation that appears to be superposed over all other minor structures. Shear indicators could not be found.

MICROSTRUCTURE

Observations and measurements

Calcite is the dominant phase in all investigated samples. Minor mineral components are quartz, feldspar, mica, pyrite and hematite. Full details are given in Table 2. These secondary components mostly define thin layers which comprise the macroscopic foliation (see Ramsay & Huber 1987, p. 591 for definitions of foliation and schistosity). In general, it is well developed together with a lineation that we interpret from field data as the stretching direction. Most samples have a predominantly symmetric microstructure; only a few (BS, RR, RS, LC) are consistently asymmetric. The microstructure of all samples is characterized by varying amounts of mechanical twinning and recrystallization of calcite.

Mechanical twinning and the formation of *e*-lamellae is the common low-temperature deformation mechanism in calcite crystals of marble tectonites (Turner 1953). In the investigated samples, it is particularly strong in larger (relic) grains and its importance decreases with an increasing amount of recrystallization (see Fig. 2). This is in accordance with experimental data presented by Schmid *et al.* (1987). The twins near the edges of the grains are frequently bent towards the direction of the macroscopic foliation and display a sigmoidal pattern (Fig. 2b). Twins nucleate at grain boundaries and propagate into the crystal, often wedging out before they reach the opposite side. In samples with asymmetric microstructures one set of twins dominates over the others and can be used as a shear indicator (in combination with the orientation of the *c*-axis; Laurent 1987). The shear sense on each twin, as deduced from the reorientation of the *c*-axis, is consistent with the macroscopic shear direction in the specimen (see Fig. 4).

Recrystallization of calcite is concentrated at grain and twin boundaries and leads to a bimodal grain size distribution by forming rims of small recrystallized grains around large relic grains (Fig. 2b). The misorientation of the recrystallized grains increases with distance from the host grain (= relic grain). In sections parallel to the lineation and perpendicular to the macroscopic foliation, the host grains display a more or less elliptical grainshape. We follow Ramsay & Huber (1987, p. 591) in referring to the alignment of long axes of the elliptical grains as schistosity. The angle, α, between the schistosity and the macroscopic foliation varies over a relatively wide range even within a single sample. There is only a weak relationship between this angle and the total strain of the grain as assessed by the aspect ratio (Fig. 5). The average aspect ratio, as well as the average angle between schistosity and foliation (as determined by optical microscopy), for the different samples are listed in Table 2.

In order to quantify the microstructural characteristics of the asymmetric samples, we measured a set of angular relationships between the macroscopic foliation *F*, the long axis of the grains (schistosity, *S*), the trace of *c*-axis [0001], and the trace of the dominant *e*-twin lamellae $\{01\bar{1}8\}$ for selected marble samples. The measured angles, shown in Fig. 6, are defined as follows:

—α is the angle between the trace of the macroscopic foliation plane and the long axis of the elliptical grainshape (= schistosity);

Table 2. Microstructural data of the investigated samples

Sample	% recrystallization	Axial-ratio of relic grains	Grainshape asymmetry (α)	Asymmetry of the $\{11\bar{2}0\}$ girdle (ω)	Grain size	Twinning	Stylolites, veins	Other minerals
Raft River (RR)	40–60	1:1 to 1:3	23°	2,4°	relics 0.6–1 mm rexx 50–300 μm	equal in relics and rexx	thin veins coated with hematite	few micas
Ruby Mountains, Secret Pass (SP)	>95	no relics	0°	4°	rexx *ca* 10 μm	no twinning	none	quartz, plagioclase, mica
Ruby Mountains, Lamoille Canyon (LC)	90	1:2 to 1:4	8°	6,9°	relics 0.3–0.7 mm rexx 30–80 μm	weak twinning in relics	none	none
Snake Ranges (SR)	20–50	1:2 to 1:3	0°	2,3°	relics 0.2–0.6 mm rexx 10 μm	strong twinning in relics	irregular veins with calcite filling	quartz
Rincon Mountains (RN)	20–30	1:1 to 1:2	0°	15,18°	relics 0.5–1 mm rexx 50–200 μm	strong twinning in relics	none	quartz, mica
Riverside Mountains (RS)	none	1:2 to 1:3	19°	5°	0.2–0.5 mm	strong twinning	s—parallel filled with hematite and calcite	none
Eastern Peninsular Ranges, Borrego Springs (BS)	none	1:2 to 1:3	27°	9,10°	0.2–0.7 mm	strong twinning	s—parallel filled with pyrite	quartz, mica
Eastern Peninsular Ranges, Palm Canyon (PC)	60–80	1:2 to 1:4	0°	4,13°	relics 1–2 mm rexx 50–100 μm	medium twinning in relics and rexx	veins filled with quartz	quartz, mica
Death Valley Region, North Funeral Mountains (FN)	90	1:1 to 1:3	0°	−1,3°	relics 0.5–1 mm rexx *ca* 10 μm	no twinning	s—parallel and discordant veins filled with calcite	quartz, pyrite
Death Valley Region, South Funeral Mountains (FS)	90	1:1 to 1:3	0°	1,5°	relics 0.5–0.8 mm rexx 30–100 μm	twinning in relics and rexx	s—parallel and irregular veins filled with quartz and pyrite	mica
Death Valley Region, Panamint Ranges (MC)	40–60	1:1 to 1:2	0°	3,4°	relics 0.5–0.8 mm rexx 30–100 μm	strong twinning in relics	discordant veins filled with calcite	quartz

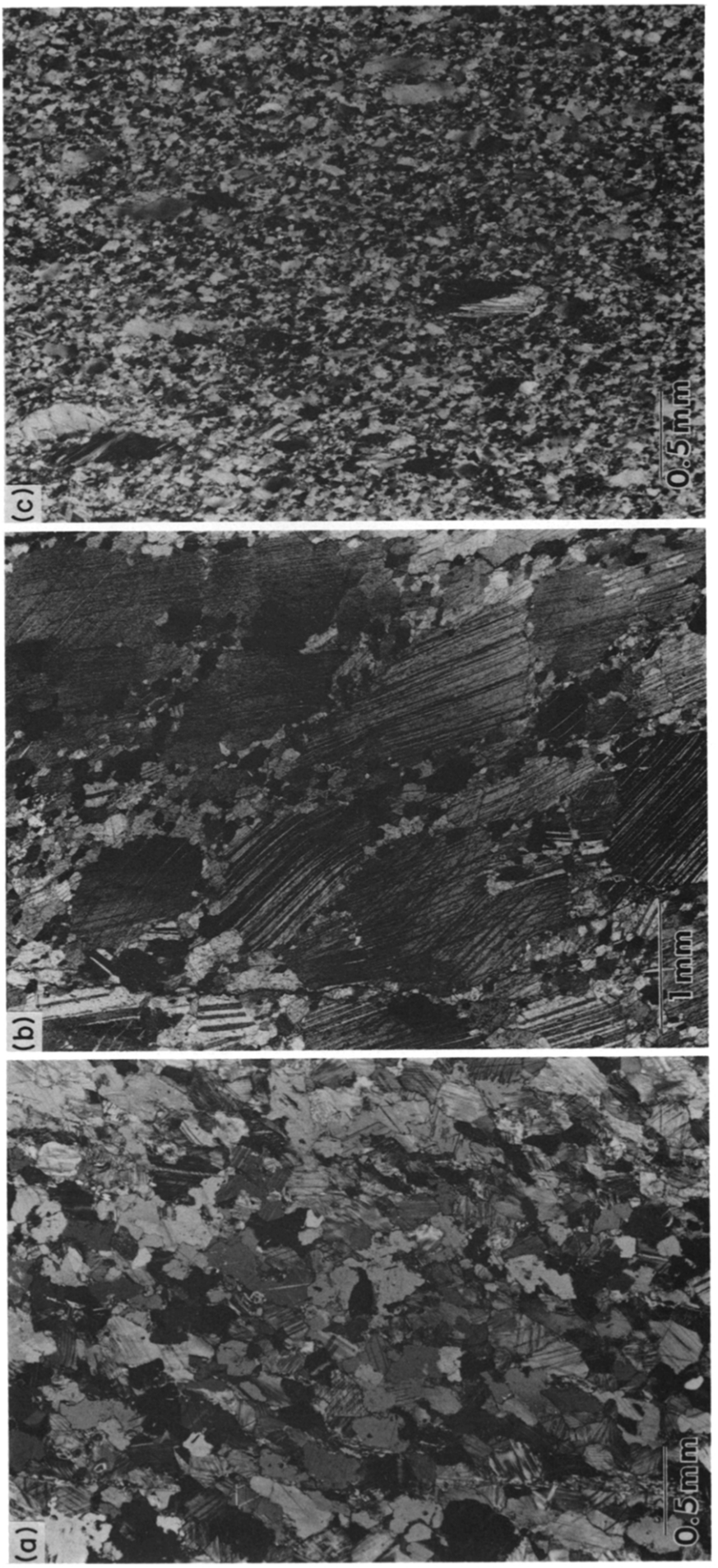

Fig. 2. Optical micrographs of the main types of microstructures. Macroscopic foliation is vertical and sections are parallel to the lineation. Sense of shear is sinistral for (a) and dextral for (b) and (c): (a) Borrego Springs (BS) (not recrystallized); (b) Raft River (RR) (partially recrystallized with relic grains); (c) Lamoille Canyon (LC) (largely recrystallized).

Fig. 3. TEM-micrographs of (a) relic grains and (b) & (c) recrystallized grains. (a) Straight dislocation lines in a relic grain of sample RR; trails of small loops are visible in the upper part of the micrograph (arrows). The double contrast of the dislocation lines is due to imaging conditions. (b) Subgrain boundaries and curved dislocations in a recrystallized grain of sample LC; the subgrain boundaries form a cell structure. (c) Microtwinning in a recrystallized grain of sample LC; notice the horizontal shear-bands indicating that the twinning occurred after the shear-band formation.

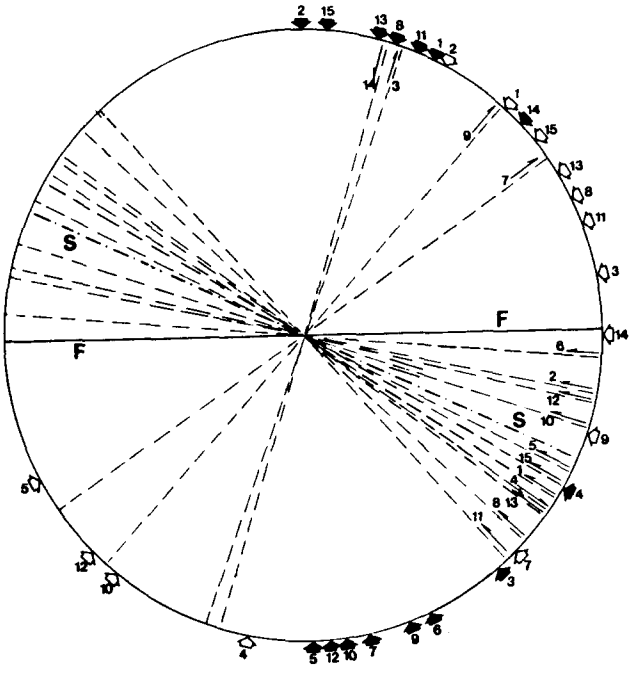

Fig. 4. Stereographic projection with the traces of twin planes (dashed) and of *c*-axes of host and twin (solid and open arrows, respectively) for sample BS 3; shear sense on each twin plane is derived from rotation of respective *c*-axis; full line indicates orientation of foliation (*F*) and dashed line shows average grain shape schistosity for bulk sample (*S*). Projection plane is parallel to the lineation and bulk shear sense is sinistral.

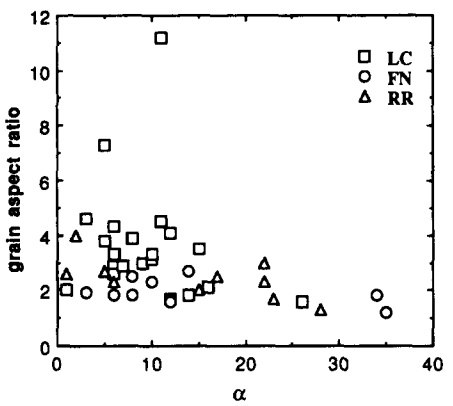

Fig. 5. Relationship between finite strain as evaluated by the aspect ratio of relic grains (ratio of long axis to short axis of grain shape) and the asymmetry of schistosity (*S*) and foliation (*F*) (=angle α) for samples from three localities.

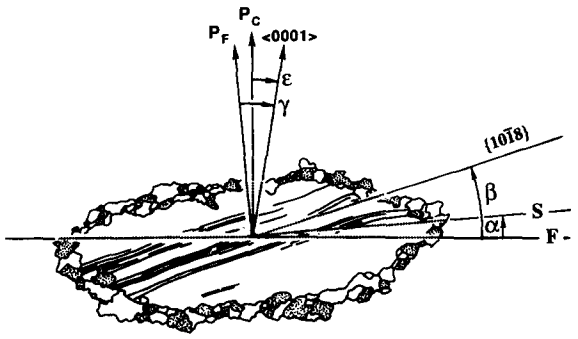

Fig. 6. Schematic drawing of typical relic grain to define the angles α, β, γ and ε. All angles are + in clockwise and − in counterclockwise direction.

—β is the angle between the trace of the foliation plane and the trace of the twin plane; we took all visible twins in each grain into account;

—ε is the angle between the normal of the trace of the foliation plane and the trace of the *c*-axis measured by the extinction position of the individual grain;

—γ is the angle between the normal to the long axis of the grain ellipse and the trace of the *c*-axis.

All relationships were measured with a flat stage petrographic microscope in ultra thin sections cut perpendicular to the macroscopic foliation and parallel to the lineation. One hundred grains were measured in each sample, and only relic grains were taken into account. From these data histograms were constructed collecting grains in angle intervals of 5° (Fig. 7).

We chose four samples for our measurements representing the main types of different microstructures that we found. The Borrego Springs (BS) samples display a medium unimodal grain size and all grains have more or less intense twinning (Fig. 2a). For this rather complicated type of microstructure with weak preferred orientation, we measured two different samples in order to identify the truly representative features. The sample from Raft River (RR) has the typical bimodal grain size distribution with large relic grains surrounded by small recrystallized grains (Fig. 2b). The sample from Lamoille Canyon (LC) is nearly completely recrystallized with only very few relic grains (Fig. 2c).

Results (Fig. 7)

We observe that the angle α between the long grain axis and the foliation is highest (25°) for the samples that show no evidence of recrystallization (BS). The peak angle decreases in more strongly recrystallized samples (20°, RR) and is smallest in the sample with only a few relic grains (5°, LC).

The angle β between the twin lamellae and the foliation is poorly defined in the BS samples but shows a definite preferred distribution in RR and LC which increases in sharpness with recrystallization. The asymmetry of this maximum of twin lamellae decreases with increasing recrystallization (from 35° (BS) to 15° (LC)).

The angle ε between traces of the *c*-axes and the foliation in the BS samples has only a weak preferred orientation which is centered normal to the foliation. RR has a strong *c*-axis maximum inclined 25° to the foliation, whereas LC displays a slightly asymmetrical peak inclined 5° to the foliation. The distributions of the *c*-axes in all samples is in good agreement with the data derived from the X-ray measurements (discussed below).

The angle γ between the long axis of the grain shape (schistosity) and the *c*-axis trace displays a weak symmetrical maximum in BS. In RR and LC samples, they show sharper distributions oblique to the schistosity, about 15° and 5°, respectively. The angle γ is smaller than ε.

The results of these measurements reveal for all samples a pronounced obliquity between the features of

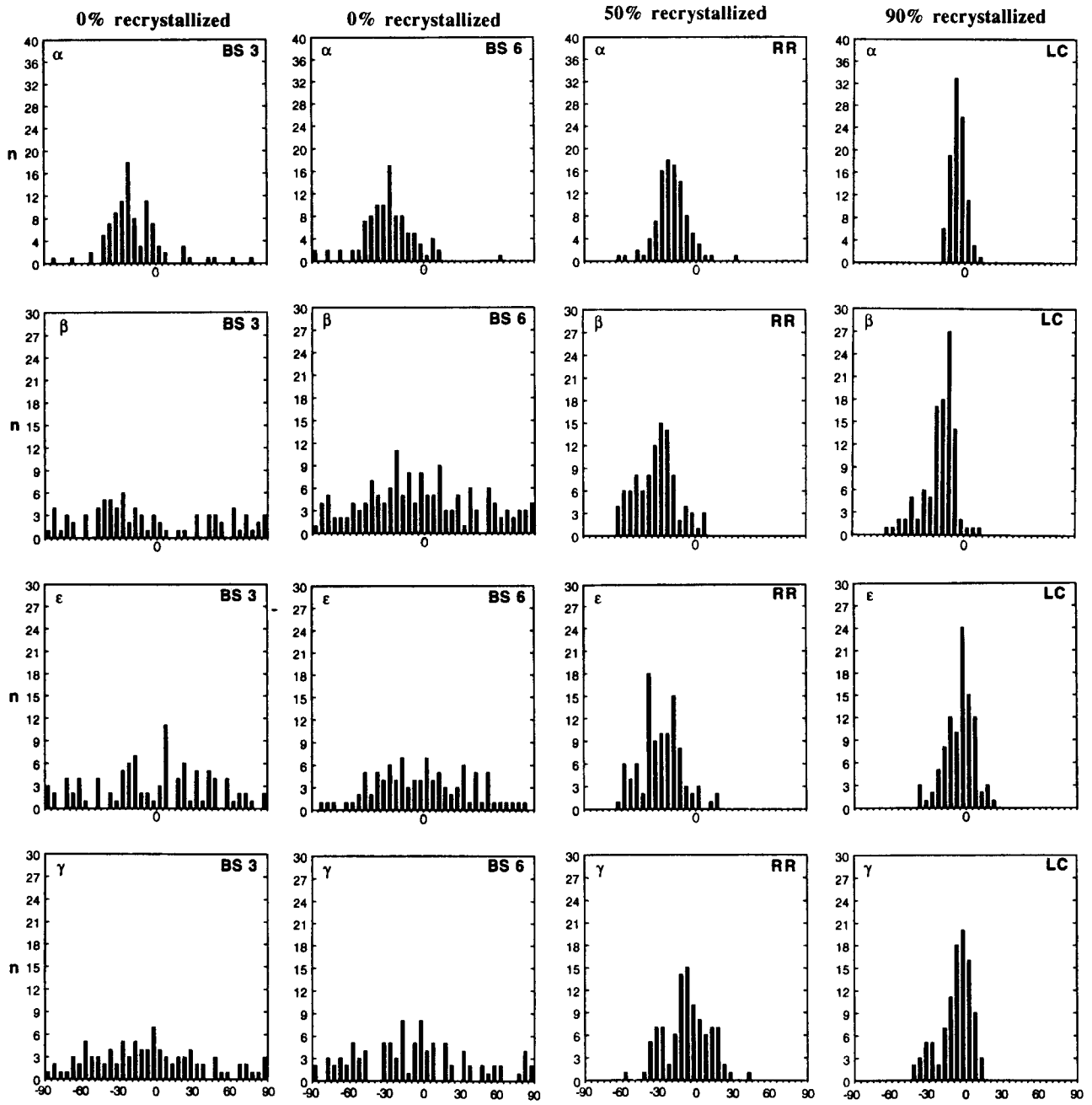

Fig. 7. Histograms with microstructural data for samples BS3, BS6, RR, LC: (a) α, (b) β, (c) γ and (d) ε. + and − refer to angles in clockwise and counterclockwise directions relative to the reference direction. For further explanation see text and Fig. 6.

single grains (*e*-lamellae, *c*-axes and elongation) and the mesoscopic structural elements for the whole rock (foliation, lineation). The obliquity of all these elements decreases with increasing recrystallization. The fabric asymmetry in these calcite mylonites resembles the *S–C* relationships described for quartz–mica mylonites by Lister & Snoke (1984). However, the development of the characteristic microstructures (especially foliation and oblique planar elements) in the deformed marbles is not very consistent, and therefore a direct correlation between structures in the two rock types is not warranted. The histograms of γ do not indicate a simple relationship between the schistosity and the *c*-axis as was found by Dietrich & Song (1983) in calcite mylonites from the western Alps. The *c*-axes in their samples were consistently aligned with the schistosity normal, independent of the bulk texture.

Transmission electron microscopy

We investigated characteristic samples (RR, LC, SR) with the transmission electron microscope (TEM) in order to determine differences in the submicroscopic structure of relic and recrystallized grains.

Characteristic for the relic grains are isolated straight dislocation lines with trails of small loops (arrows, Fig. 3a). Relatively few microtwins were found compared to the abundance of twins visible in the light microscope. The trails of loops are interpreted as products of movement of dipoles. In a particular grain the sense of

movement is the same for all observed trails. Dislocation densities are about 2×10^8 cm^{-2}. In the small recrystallized grains we observed fairly high concentrations of tangled dislocations and subgrain boundaries which make it difficult to determine the dislocation density (Fig. 3b). We estimate the dislocation density to be higher than 10^9 cm^{-2}. The dislocation lines are often curved and the subgrains typically have a cell structure. The new grains have obviously been deformed after recrystallization. Locally intensive microtwinning was observed in these newly recrystallized grains which is offset by intersecting shearbands (see Fig. 3c). The twin lamellae are up to 0.1 μm wide and compose about 10% of the volume. Such twinned regions however, are rather exceptional.

X-RAY TEXTURE ANALYSIS

Measurement of pole figures and calculation of the orientation distribution function

Slabs from oriented hand specimens were cut perpendicular to the macroscopic foliation F and parallel to the lineation L. On these slabs, incomplete pole figures for several diffraction peaks were measured with a modified Norelco X-ray pole figure goniometer in reflection geometry (see Wenk 1985 for details). The pole figures were continuously scanned on a spiral path with a 5° divergence, and samples were translated to obtain a better grain average. Intensities were measured for 100 s covering about a 3° spiral increment. Defocusing of the incident beam as a function of sample tilt was corrected using a limestone standard with a random texture. Due to defocusing, measurements between 80° and 90° were not very reliable and were not used in the normalization, data processing or plotting.

For most samples we relied only on $\{11\bar{2}0\}$ pole figures which are easy to measure, but for three selected samples (Lamoille Canyon (LC1), Funeral Mountains (FN2) and Snake Ranges (SR3)) the three-dimensional orientation distribution (ODF) was calculated using the WIMV algorithm (Matthies *et al.* 1988) from three incomplete pole figures of the lattice planes $\{11\bar{2}0\}$, $\{10\bar{1}4\}$ and $\{20\bar{2}2\}$ (Fig. 8). In contrast to pole figures which plot only the orientation distribution of a single lattice direction with respect to the sample co-ordinates, the ODF is a more complete texture representation which relates the crystallite co-ordinate system and the sample reference frame. Two right-handed co-ordinate systems need to be specified for the ODF representation. In analogy to earlier studies (Wenk *et al.* 1987), the crystal co-ordinate system is chosen as: $X^c = [2\bar{1}\bar{1}0]$, the crystal a-axis; $Z^c = [0001]$, the crystal c-axis, and Y^c normal to these two directions. The sample co-ordinate system is defined as X^s, the lineation (right on pole figure), Y^s the normal to the microscopic foliation (top on pole figure) and Z^s the intermediate fabric direction (center on pole figure). We used the Roe (1965) convention of Euler angles and represent the ODF in the recently introduced $\sigma = (\Phi + \Psi)/2$ sections rather than Φ sections in equal-area projection (Fig. 9). The σ-sections are advantageous because of minimal distortion (Helming *et al.* 1988). The two-dimensional sections of the three-dimensional ODF may be visualized as orientation distributions of c-axes with respect to different a-axes orientations (Wenk & Kocks 1987). The last plot of the ODF sections is an average over all sections, and represents a standard c-axis pole figure.

The calculation of the ODF is important in this study for three reasons. First, recent work that quantitatively relates calcite textures to the strain path is based on a comparison of natural, experimental and simulated textures in ODF space (Wenk *et al.* 1987). Second, the ODF enables the calculation of pole figures of any desirable lattice direction. In particular, c-axis pole figures of the samples under study may be plotted for comparison with the microstructure. The {0006} X-ray reflection is weak and is difficult to measure because of its proximity to the intense $\{10\bar{1}4\}$ reflection. Finally, intensity measurements are affected by a number of factors such as sample heterogeneity and the presence of impurities such as quartz and calcium silicate minerals. The ODF calculation also allows us to assess the quality of the pole figure data with quantitative error criteria. The significance of minor features such as variations of a-axis densities in the foliation plane can be evaluated. Agreement between the measured and the recalculated pole figures provides confidence in the measured data.

Pole figures from each of the three sites are similar (Fig. 8). The $\{11\bar{2}0\}$ pole figures display a symmetric to slightly asymmetric great circle girdle that is nearly parallel to the mesoscopic foliation F. The $\{10\bar{1}4\}$ poles are within two small circle girdles that are distributed about the pole normal to the $\{11\bar{2}0\}$ girdle. The $\{20\bar{2}2\}$ poles form a broad great circle girdle that is parallel to the $\{11\bar{2}0\}$ girdle, and contains two point maxima that are bisected by the external fabric co-ordinates. The {0006} poles (not used in the ODF calculations) form a point maximum normal to the $\{11\bar{2}0\}$ girdle. There is excellent agreement between the calculated and measured pole figures in terms of their geometry and intensity, which is also expressed in good RP-values (Matthies *et al.* 1988).

The obliquity of the $\{11\bar{2}0\}$ girdle is described by the angle ω between the girdle and the foliation F. For triclinic pole figures, where the great circle girdle does not intersect the center of the pole figure (sample co-ordinate Z^s), the angle ω is measured between F and the intersection of the girdle and the edge of the pole figure.

Results

The ODFs of each of the three samples in Fig. 9 compare favorably with the low-temperature texture types described by Wenk *et al.* (1987). The high peak maxima in {0001} pole figures (between 5.0 and 10 multiples of a random distribution, m.r.d.) imply that the finite strain exceeded 30% shortening. Since pole figures and microstructures are similar, it is reasonable

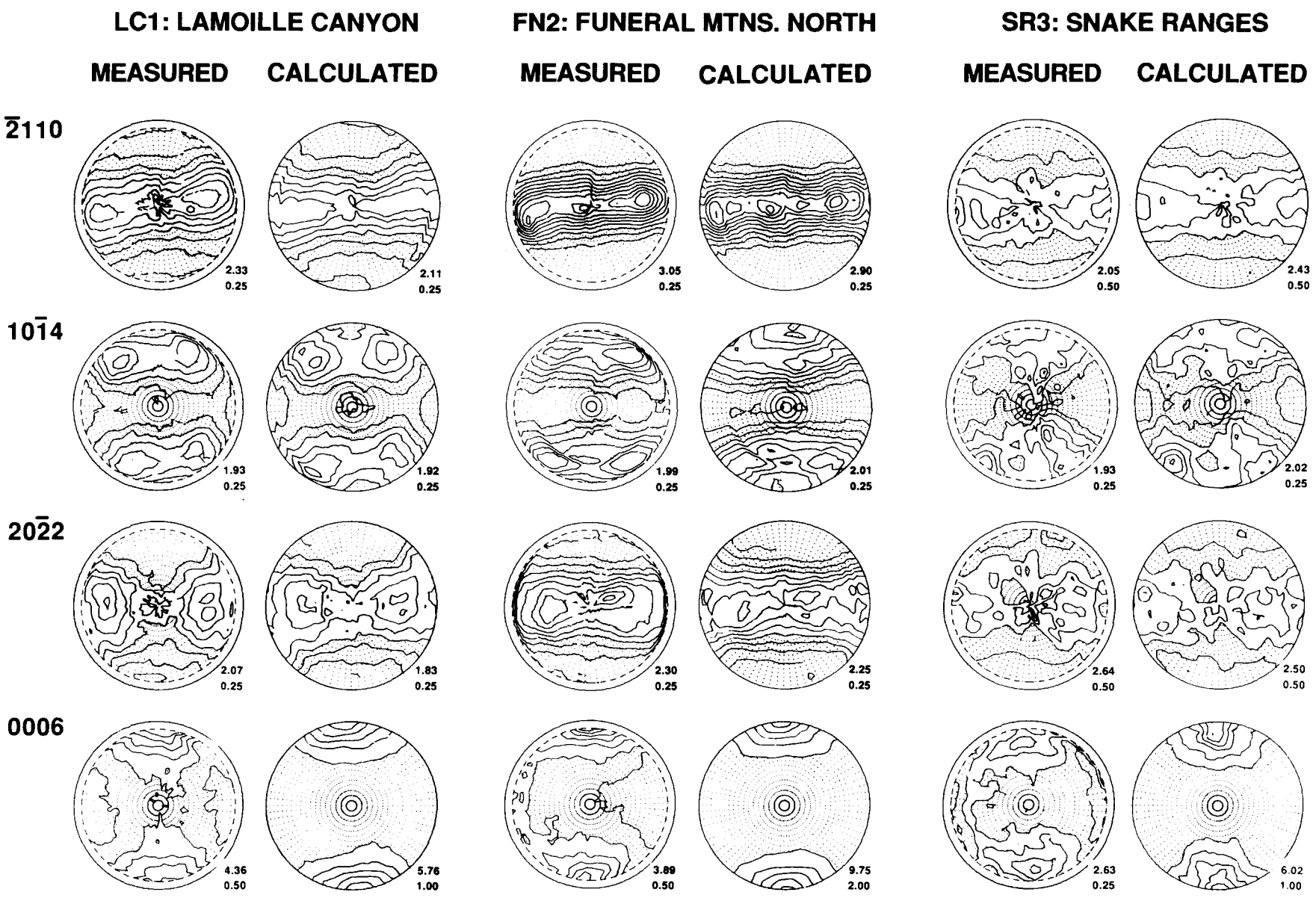

Fig. 8. Measured and recalculated pole figures for LC1, FN2 and SR3. Measured {0006} partial pole figures were not used in the ODF calculations. Upper-hemisphere equal-area projection is perpendicular to the foliation and parallel to the lineation (both in E–W, same as in Fig. 10). Maximum intensity and contour interval are shown at the lower right of each pole figure. Areas with intensities below 1.0 m.r.d. (= random) are decorated by concentric rings of points with angular spacings of 5°.

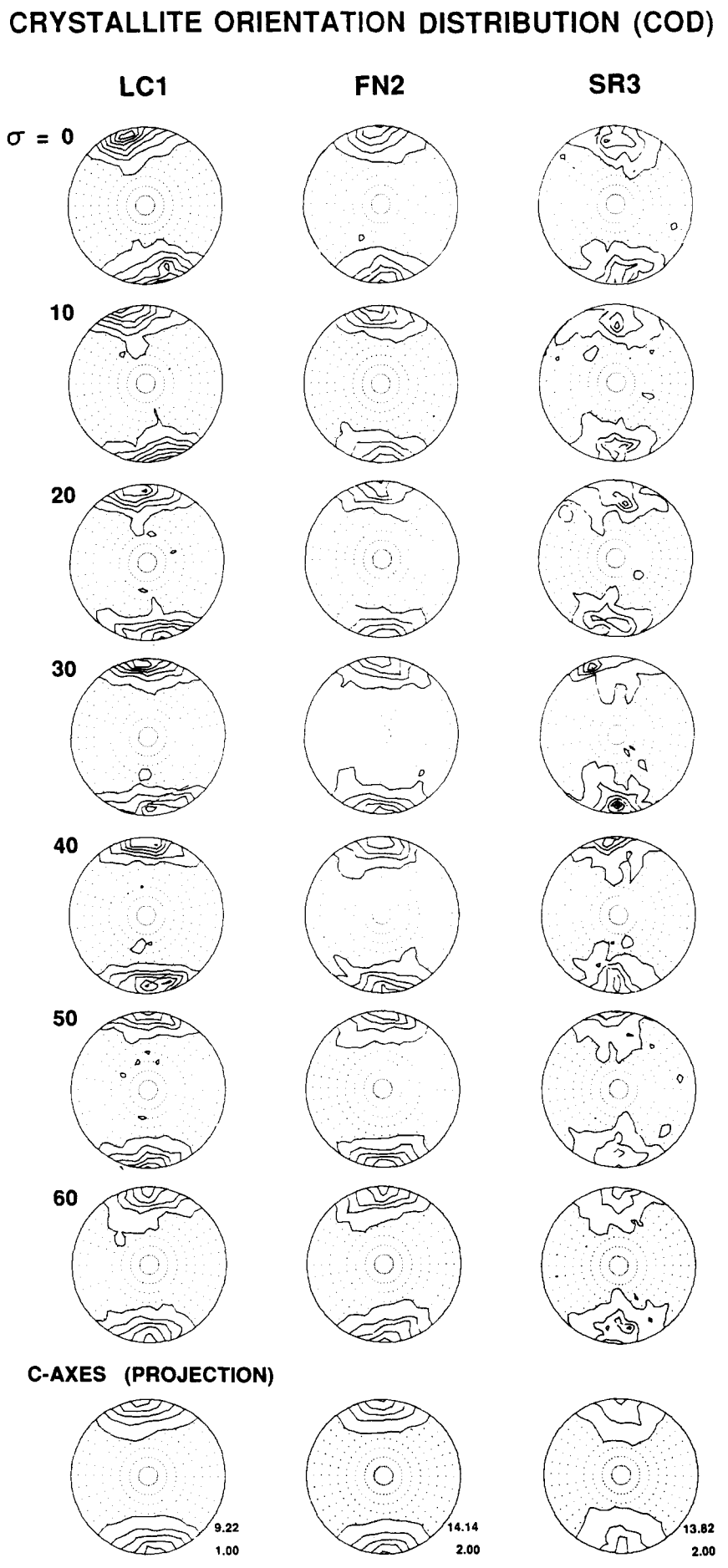

Fig. 9. ODF in σ-sections for LC1, FN2 and SR3.

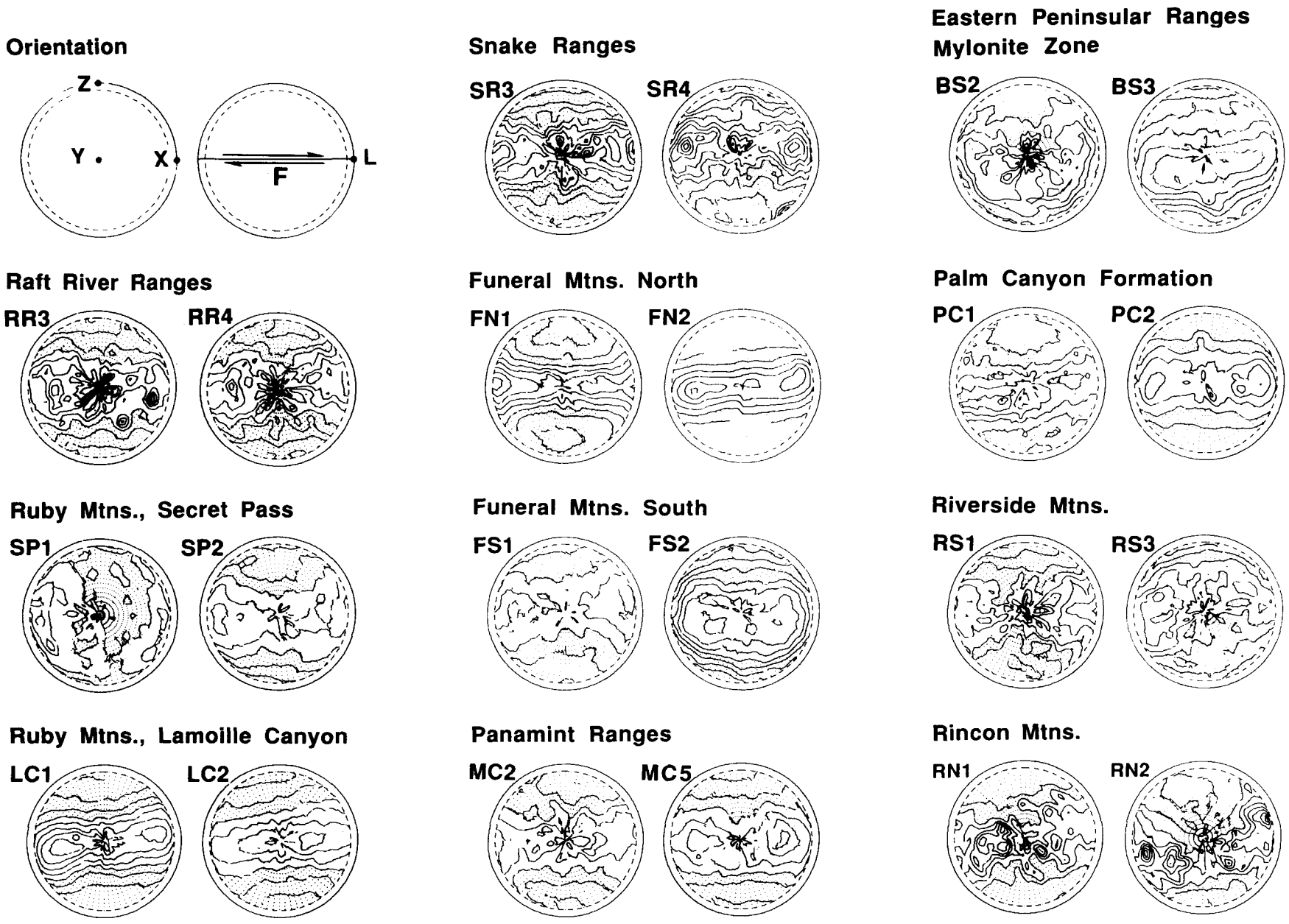

Fig. 10. $\{11\bar{2}0\}$ pole figures (upper-hemisphere, equal area) from each of the eleven sample localities. Contours levels are in 0.25 m.r.d. steps. The field of values below 1.0 m.r.d. (= random) is decorated by concentric rings of points with angular spacings of 5°. The top left diagrams specify the internal co-ordinate system used in the analysis ($X^sY^sZ^s$) and the macroscopic co-ordinates, foliation F and lineation L. If deformation in simple shear occurred, the foliation plane, defined by compositional banding, is the most likely macroscopic shear plane. Pole figures are presented with a dextral sense of shear, determined by independent shear criteria in the field.

to assume that the lattice preferred orientation and the microscopic fabric are related to the last major phase of deformation in each of the respective areas, and do not represent local last-stage deformation events.

Visual inspection of Fig. 10 reveals three common features among the sampling sites. The first is a consistency in the texture pattern. Each pole figure is defined by a great circle $\{11\bar{2}0\}$ girdle that, in general, intersects the Z^s sample axis. About half of the pole figures are smooth and regular, others are more heterogeneous with spurious maxima which can be attributed to large grain size and contributions from silicate inclusions (the quartz and calcite $\{11\bar{2}0\}$ reflections are at very similar Bragg angles). In those samples with a reasonably smooth girdle, there are generally subsidiary concentrations at 50–60°.

The second common feature is a similarity in the symmetry of the pole figures with respect to the chosen sample axes. Most are nearly orthorhombic with $\{11\bar{2}0\}$ girdles being tilted less than 10° from the macroscopic foliation plane F. In some samples (BS2 and 3, SR4, RN2, FS2) the girdle is considerably (up to 30°) tilted around Y^s (triclinic pole figures), indicating that the deformation geometry deviated from plane strain conditions.

The third common feature of the pole figures is that the sense of asymmetry around Z^s, even though small, is the same for all samples. The $\{11\bar{2}0\}$ girdles are slightly rotated against the sense of shear implied from independent shear criteria.

DISCUSSION

Texture patterns in these highly deformed marbles have been surprisingly uniform in spite of very different degrees of recrystallization. They are characteristic of the calcite low-temperature texture that has been observed below 300–400°C in experimentally deformed, fine-grained limestone (Wenk *et al.* 1987). High-temperature textures were not found in any of the samples measured, and so far there have been no reports of such in naturally deformed carbonate rocks. Such low-temperature textures develop at conditions where r^--slip and e^+-twinning are dominantly active (Takeshita *et al.* 1987). The high, nearly orthorhombic, symmetry has been unexpected because it is indicative of coaxial deformation. Wenk *et al.* (1987) provided a method to estimate the contribution of simple shear to the total strain, based on the angle between the c-axis maximum in the pole figure and the pole to the macroscopic shear plane. This angle is equivalent to the angle ω between the $\{11\bar{2}0\}$ girdle and the shear plane which has been introduced above. In these rocks ω never exceeds 18°. Values for individual samples are listed in Table 2.

A determinative chart (Fig. 11) can be used if the macroscopic shear plane is known and if deformation occurs by the above described mechanisms. The chart was obtained from polycrystal plasticity simulations

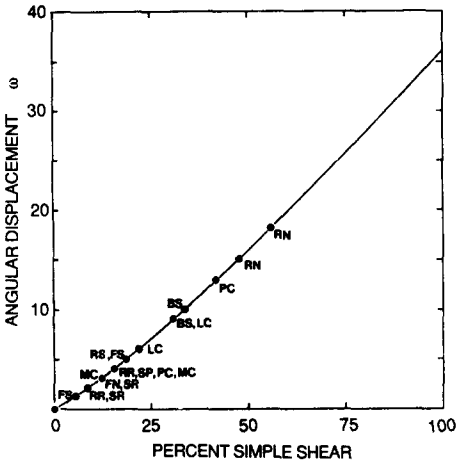

Fig. 11. Determinative diagram to estimate percentage of simple shear deformation from the asymmetry of the $\{11\bar{2}0\}$ girdle with the macroscopic foliation F, and ω (from Wenk *et al.* 1987).

based on the viscoplastic self-consistent theory (e.g. Tomé *et al.* 1991). These calculations indicate that in simple shear the a-axis girdle is inclined 37° to the shear plane, and the orientation of the girdle does not change with increasing shear strain. In pure shear the girdle lies perpendicular to the direction of shortening. For a strain path which is intermediate between simple and pure shear—as described by a displacement gradient tensor $(D_{11}\ D_{12})\ (0 - D_{11})$—the angle ω varies almost linearly with the amount of simple shear ($\% = 100\ D_{12}/(2D_{11} + D_{12})$) from 0° to 37°. The ω angles in the samples described here range from 0° to 18° (Table 2), which implies simple shear components from 0 to 40%.

What is the influence of recrystallization in these samples which occurred mainly by nucleation of new grains along twin and grain boundaries? Dislocation structures in relic and recrystallized grains are similar; both are deformed, indicative of dynamic recrystallization. Also, the textures of more or less recrystallized samples are similar, suggesting that there were no major strain path changes during tectonic deformation of these marble samples. Since the asymmetry ω of the texture does not change with increasing deformation, recrystallized grains which enter the deformation process at a later stage rotate into the same maximum and do not change in angular position. If there would have been a change in strain path, such as pure shear deformation, recrystallization followed by simple shear deformation, one would expect a texture consistent with simple shear, at least after a total strain of 30–50%.

The microstructure of the investigated samples is predominantly symmetric and could be the result either of a pure shear deformation or of an extremely large simple shear deformation. The few samples, which display asymmetric microstructures and were analyzed more closely, have an irregular pattern if compared with their respective textures.

The Borrego Springs samples have the highest microstructural asymmetry ($\alpha \approx 27°$) and a relatively high $\omega(\approx 10°)$ in the texture, whereas the sample from Raft

River is similarly asymmetric in the microstructure ($\alpha \approx 23°$) but possesses a fairly symmetric texture ($\omega \approx 4°$). The Lamoille Canyon samples have an asymmetric texture ($\omega \approx 9°$) and a slightly asymmetric microstructure ($\alpha \approx 8°$). These inconsistencies may be due to the strong twinning in the relic grains which causes a decrease in the strength of the preferred orientation because it rotates the *c*-axis away from the point maximum in a sense opposite to the shear on the twin plane (Fig. 4). Furthermore the microstructural data (Fig. 7) indicate a close relationship between twinning and grainshape (angles α and β) whereas the preferred orientation of the *c*-axes (angles ε,γ) is not as clearly related to the grainshape. Microstructure and texture therefore might be related to different deformation stages, i.e. the bulk texture is the result of an older pure shear deformation, whereas the microstructure is produced by a younger simple shear deformation which was dominantly accomplished by twinning. Twinning is strongly developed in most of the samples (see Table 2) and may account for a significant amount of the overall strain. Dynamic recrystallization may produce a spread of orientations ± around the point maximum of the deformation texture (e.g. Friedman & Higgs 1981, de Bresser 1989), but does not significantly change the overall texture type. The effect on the determination of the angle ω is therefore considered to be only minor. Recrystallization also may affect the grain shape and therefore the direction and length of the long axis of an ellipsoidal relic grain (angle α).

In summary, our results suggest that in marbles of core complexes in the western United States and associated tectonic units which we studied, the non-coaxial component is relatively small. The textures contrast with those from thrust nappes of low metamorphic grade in the Alps (Schmid *et al.* 1981, Dietrich & Song 1984, Dietrich & Durney 1986, Ratschbacher *et al.* 1991) where asymmetric calcite fabrics are common and the asymmetry is systematically related to the strain distribution expected in a spreading–gliding nappe (e.g. Merle 1989). A notable exception in these Alpine carbonate rocks is a very highly deformed calcite mylonite along the thrust contact in the Graz Paleozoic which displays a well-developed symmetrical fabric (Ratschbacher *et al.* 1991). In this paper the pure shear deformation in extreme strain situations is attributed to the fact that pure shear in calcite is energetically favored over simple shear (Takeshita *et al.* 1987, Wenk *et al.* 1987). If heterogeneous deformation is possible, this mode may be preferred, even though on a large scale, the bulk of the deformation may occur by shearing.

A similar situation could conceivably exist in carbonate rocks from the core complexes. Carbonate rocks could deform heterogeneously but coaxially in an otherwise dominantly non-coaxial shear zone; however, fabric studies on quartzites describe symmetric (e.g. Compton 1980, Lee *et al.* 1987) or moderately asymmetric textures (Lister & Snoke 1984, Davis *et al.* 1986, 1987). This would imply that the core complexes deformed primarily by coaxial deformation (e.g. Miller *et al.* 1983, Lee *et al.* 1987), rather than simple shear deformation in a large shear zone (e.g. Wernicke 1981, 1983, 1985, Wernicke & Burchfiel 1982). The relatively small component of simple shear in the samples is expressed in the slight asymmetry of the *a*-axis girdles relative to the macroscopic shear plane.

In conclusion we have demonstrated that calcite fabrics in deformed marble contribute important information for the determination of the overall strain path. X-ray pole figure analysis on oriented specimens was an efficient method to measure preferred orientation. A survey of marbles from metamorphic core complexes suggests predominantly coaxial deformation which could originate from crustal thinning. Slight asymmetries in pole figures permit the determination of the local sense of shear.

Acknowledgements—We are appreciative to R. R. Compton, G. H. Davis, E. G. Frost, P. B. Gans, K. A. Howard and E. L. Miller for introducing us to some of the field areas covered in this study. Financial support was provided through grants from NSF EAR9017237 and IGPP-LANL.

REFERENCES

Armstrong, R. L. 1982. Cordilleran core complexes from Arizona to southern Canada. *Am. Rev. Earth & Planet Sci.* **10**, 129–154.

Compton, R. R. 1975. Geologic map of the Park Valley quadrangle, Box Elder County, Utah and Cassia County, Idaho. *U.S. geol. Surv. Miscell. Geol. Invest.* Map I-873.

Compton, R. R. 1980. Fabrics and strains in quartzites of a metamorphic core complex, Raft River Mountains, Utah. *Mem. geol. Soc. Am.* **153**, 385–398.

Compton, R. R., Todd, V. R., Zartman, R. E. & Naeser, C. W. 1977. Oligocene and Miocene metamorphism, folding, and low-angle faulting in northwestern Utah. *Bull. geol. Soc. Am.* **88**, 1237–1250.

Coney, P. J. 1973. Non-collision tectogenesis in western North America. In: *Implications of Continental Drift to Earth Sciences* (edited by Tarling, D. H. & Runcorn, S. H.). New York, Academic Press, 713–717.

Coney, P. J. 1980. Cordilleran metamorphic core complexes: An overview. *Mem. geol. Soc. Am.* **153**, 7–31.

Crittenden, M. D., Coney, P. J. & Davis, G. H. (editors). 1980. Tectonic significance of metamorphic core complexes of the North American Cordillera. *Mem. geol. Soc. Am.* **153**.

Davis, G. A., Lister, G. S. & Reynolds, S. J. 1986. Structural evolution of the Whipple and South mountains shear zones, southwestern United States. *Geology* **14**, 7–10.

Davis, G. H. 1975. Gravity-induced folding off a gneiss dome complex, Rincon Mountains, Arizona. *Bull. geol. Soc. Am.* **86**, 979–990.

Davis, G. H. 1983. Shear zone model for the origin of metamorphic core complexes. *Geology* **11**, 342–347.

Davis, G. H., Gardulski, A. F. & Lister, G. S. 1987. Shear zone origin of quartzite mylonite and mylonitic pegmatite in the Coyote Mountains metamorphic core complex, Arizona. *J. Struct. Geol.* **9**, 289–298.

de Bresser, J. H. P. 1989. Calcite *c*-axis textures along the Gavarnie thrust zone, central Pyrenees. *Geologie Mijnb.* **68**, 367–375.

Dietrich, D. & Durney, D. W. 1986. Change of direction of overthrust shear in the Helvetic nappes of western Switzerland. *J. Struct. Geol.* **8**, 389–398.

Dietrich, D. & Song, H. 1983. Calcite fabrics in a natural shear environment, the Helvetic nappes of western Switzerland. *J. Struct. Geol.* **6**, 19–32.

Erskine, B. G. 1986. Mylonitic deformation and associated low angle faulting in the Eastern Peninsular Ranges Mylonite Zone, Southern California. Unpublished Ph.D. thesis, University of California, Berkeley.

Erskine, B. G. & Wenk, H. R. 1985. Evidence for Late Cretaceous crustal thinning in the Santa Rosa mylonite zone, southern California. *Geology* **13**, 274–277.

Friedman, M. & Higgs, N. G. 1981. Calcite fabrics in experimental shear zones. *Am. Geophys. Un. Geophys. Monogr.* **24**, 11–27.

Frost, E. G. 1977. Mid-Tertiary, gravity-induced deformation in Happy Valley, Pima and Cochise Counties, Arizona. Unpublished M.S. thesis, University of Arizona, Tucson.

Gans, P. & Miller, E. L. 1984. Geologic and geophysical constraints on the geometry of crustal extension in the east Basin and Range province. *Geol. Soc. Am. Abs.* **16**, 515.

Goodwin, L. B. & Renne, P. R. 1991. Effects of progressive mylonitization on Ar retention in biotites from the Santa Rosa mylonite zone, California and thermochronologic implications. *Contr. Miner. Petrol.* **108**, 283–297.

Haxel, G., Tosdal, R. M., May, D. J. & Wright, J. E. 1984. Latest Cretaceous and Early Tertiary orogenesis in south central Arizona—Thrust faulting, regional metamorphism, and granitic plutonism. *Bull. geol. Soc. Am.* **95**, 631–653.

Helming, K., Matthies, S. & Vinel, G. W. 1988. ODF representation by means of σ-sections. In: *Proc. 8th International Conference on Textures in Materials (ICOTOM)* (edited by Kallend, J. S. & Gottstein, G.). The Metallurgical Society, Warrendale, Pennsylvania, 55–60.

Howard, K. A. 1966. Structure of the metamorphic rocks of the northern Ruby Mountains, Nevada. Unpublished Ph.D. thesis, Yale University, New Haven.

Howard, K. A. 1968. Flow direction in triclinic folded rocks. *Am. J. Sci.* **266**, 758–765.

Howard, K. A. 1980. Metamorphic infrastructure in the northern Ruby Mountains, Nevada. *Mem. geol. Soc. Am.* **153**, 335–347.

Laurent, P. 1987. Shear-sense determination on striated faults from *e* twin lamellae in calcite. *J. Struct. Geol.* **9**, 591–595.

Lee, J., Miller, E. L. & Sutter, J. F. 1987. Ductile strain and metamorphism in an extensional tectonic setting: a case study from the northern Snake Range, Nevada, U.S.A. In: *Continental Extensional Tectonics* (edited by Coward, M. P., Dewey, J. F. & Hancock, P. L.). *Spec. Publs geol. Soc. Lond.* **28**, 267–298.

Lingrey, S. H. 1982. Structural geology and tectonic evolution of the northeastern Rincon Mountains, Cochise and Pima Counties, Arizona. Unpublished Ph.D. thesis, University of Arizona, Tucson.

Lister, G. S. & Davis, G. A. 1989. The origin of metamorphic core complexes and detachment faults formed during Tertiary continental extension in the northern Colorado River region. *J. Struct. Geol.* **11**, 65–94.

Lister, G. S. & Snoke, A. W. 1984. S–C mylonites. *J. Struct. Geol.* **6**, 617–638.

Lyle, J. H. 1982. Interrelationship of Late Mesozoic thrust faulting and Mid-Tertiary detachment faulting in the Riverside Mountains, Southeastern California. Unpublished Ms. thesis, San Diego State University, California.

Matthies, S., Wenk, H.-R. & Vinel, G. W. 1988. Some basic concepts of texture analysis and comparison of three methods to calculate orientation distribution functions from pole figures. *J. appl. Cryst.* **21**, 285–304.

Merle, O. 1989. Strain models within spreading nappes. *Tectonophysics* **165**, 57–71.

Miller, E. L., Gans, P. B. & Garing, J. 1983. The Snake Range décollement: an exhumed mid-Tertiary brittle ductile transition. *Tectonics* **2**, 239–263.

Miller, E. L., Gans, P. B. & Lee, J. 1987. The Snake Range décollement. *G.S.A. Decade of North American Geology Field Trip Guide to the Western U.S., Cordilleran Section*, 77–82.

O'Brien, D. K., Wenk, H. R., Ratschbacher, L. & Zhendong, Y. 1987. Preferred orientation of phyllosilicates in phyllonites and ultramylonites. *J. Struct. Geol.* **9**, 719–730.

Ramsay, J. G. & Huber, M. I. 1987. *The Techniques of Modern Structural Geology, Volume 2: Folds and Fractures.* Academic Press, London.

Ratschbacher, L., Wenk, H. R. & Sintubin, M. 1991. Calcite textures: examples from nappes with strain-history partitioning. *J. Struct. Geol.* **13**, 369–384.

Rehrig, W. A. & Reynolds, S. J. 1980. Geologic and geochronologic reconnaissance of northwest trending zone of metamorphic core complexes in southern and western Arizona. *Mem. geol. Soc. Am.* **153**, 131–157.

Roe, R. J. 1965. Description of crystallite orientation in polycrystalline materials. II. General solution to pole figure inversion. *J. appl. Phys.* **36**, 2024–2031.

Schmid, S. M., Casey, M. & Starkey, J. 1981. The microfabric of calcite tectonites from the Helvetic nappes (Swiss Alps). In: *Thrust and Nappe Tectonics* (edited by McClay, K. & Price, J. J.). *Spec. Publs geol. Soc. Lond.* **9**, 151–158.

Schmid, S. M., Panozzo, R. & Bauer, S. 1987. Simple shear experiments on calcite rocks: rheology and microfabric. *J. Struct. Geol.* **9**, 747–778.

Sharp, R. V. 1979. Some characteristics of the Eastern Peninsular Ranges mylonite zone. In: *Proceedings VIII Conference Analysis of Actual Fault Zones in Bedrock. U.S. geol. Surv. Open-file Rep.* **79-1239**, 258–267.

Simpson, C. 1984. Borrego Springs–Santa Rosa mylonite zone: A late Cretaceous west directed thrust fault in Southern California. *Geology* **12**, 8–11.

Simpson, C. & Schmid, S. M. 1983. An evaluation of criteria to deduce the sense of movement in sheared rocks. *Bull. geol. Soc. Am.* **94**, 1281–1288.

Snoke, A. W. 1980. Transition from infrastructure to suprastructure in the northern Ruby Mountains, Nevada. *Mem. geol. Soc. Am.* **153**, 287–333.

Snoke, A. W. & Howard, K. A. 1984. Geology of the Ruby Mountains–East Humboldt Range, Nevada: A Cordilleran metamorphic core complex. In: *Western Geological Excursions* (edited by Lintz, J.). Mackay School of Mines, Reno, Nevada, Fieldtrip Guide Book 4, 260–304.

Takeshita, T., Tomé, C., Wenk, H. R. & Kocks, U. F. 1987. Single crystal yield surface for trigonal lattices: Application to texture transitions in calcite polycrystals. *J. geophys. Res.* **92**, 3917–3930.

Takeshita, T. & Wenk, H. R. 1988. Plastic Anisotropy and geometrical hardening in quartzites. *Tectonophysics* **149**, 345–361.

Todd, V. R., Erskine, B. G. & Morton, D. M. 1988. Metamorphic and tectonic evolution of the northern Peninsular Ranges batholith, southern California. In: *Metamorphism and Crustal Evolution of the Western United States* (edited by Ernst, W. G.). Prentice-Hall, Englewood Cliffs, New Jersey, 895–937.

Tomé, C., Wenk, H. R., Canova, G. & Kocks, U. F. 1991. Simulations of texture development in calcite: comparison of polycrystal plasticity theories. *J. geophys. Res.* **96**, 11,865–11,875.

Turner, F. J. 1953. Nature and dynamic interpretation of deformation lamellae in calcite of three marbles. *Am. J. Sci.* **25**, 276–298.

Wenk, H.-R. (editor) 1985. *Preferred Orientation in deformed Metals and Rocks; An Introduction to Modern Texture Analysis.* Academic Press, London.

Wenk, H.-R. & Kocks, U. F. 1987. The representation of orientation distributions. *Metall. Trans.* **18A**, 1083–1092.

Wenk, H.-R. & Pannetier, J. 1990. Texture development in deformed granodiorites from the Santa Rosa mylonite zone. *J. Struct. Geol.* **12**, 177–184.

Wenk, H.-R., Takeshita, T., Bechler, E., Erskine, B. G. & Matthies, S. 1987. Pure shear and simple shear calcite textures. Comparison of experimental, theoretical and natural data. *J. Struct. Geol.* **9**, 731–745.

Wernicke, B. 1981. Low angle normal faults in the Basin and Range province: nappe tectonics in an extending orogen. *Nature* **291**, 645–648.

Wernicke, B. 1983. Evidence for large-scale simple shear of the continental lithosphere during extension, Arizona and Utah. *Geol. Soc. Am. Abs.* **15**, 310–311.

Wernicke, B. 1985. Uniform-sense normal simple shear of the continental lithosphere. *Can. J. Earth Sci.* **22**, 108–126.

Wernicke, B. & Burchfiel, B. C. 1982. Modes of extensional tectonics. *J. Struct. Geol.* **4**, 105–115.

Wernicke, B. P., Hodges, K. V. & Walker, J. D. 1986. Geological setting of the Tucki Mountain area, Death Valley National Monument, California. In: *Mesozoic and Cenozoic Structural Evolution of Selected Areas, East-Central California* (edited by Dunee, G. C.). *Field Trip Guidebook of the 82nd Annual G.S.A. Meeting, Cordilleran Section* **2**, 67–80.

White, S. H., Burrows, S. E., Carreras, J., Shaw, N. D. & Humphreys, F. J. 1980. On mylonites in ductile shear zones. *J. Struct. Geol.* **2**, 175–187.

Wust, S. L. 1986. Regional correlation of extension directions in Cordilleran metamorphic core complexes. *Geology* **14**, 828–830.